# Enantioselective Modification of Sulfonamides and Sulfonamide-Containing Drugs via Carbene Organic Catalysis

Runjiang Song[+][a], Yingguo Liu[+][a], Pankaj Kumar Majhi[+][a], Ng Pei Rou[a], Lin Hao[a], Jun Xu[b,a], Weiyi Tian*[b], Long Zhang[c], Hongmei Liu[c], Xinglong Zhang*[d], Yonggui Robin Chi*[a,e]

[a]     Division of Chemistry & Mathematical Science, School of Physical & Mathematical Sciences, Nanyang Technological University, Singapore 637371, Singapore
Email: robinchi@ntu.edu.sg
[b]     Guizhou University of Traditional Chinese Medicine, Guiyang 550025, China
Email: tianweiyi@gzy.edu.cn
[c]     Institute of Nervous System Diseases, Xuzhou Medical University, Xuzhou 221002, P. R. China
[d]     Institute of High Performance Computing, A*STAR (Agency for Science, Technology and Research), 138632, Singapore
Email: zhang_xinglong@ihpc.a-star.edu.sg
[e]     Key Laboratory of Green Pesticide and Agricultural Bioengineering,Ministry of Education, Guizhou University, Huaxi District, Guiyang 550025, China
[+]     These authors contributed equally to this work.

# V Computational Methods

Geometry optimizations for conformational sampling in the gas phase were carried out using the GFN1-xTB method[1] as implemented in Entos Qcore Version 0.7.[2] The resulting cluster structures were further optimized using global hybrid functional M06-2X[3] with Karlsruhe-family basis set of double-$\zeta$ valence def2-SVP[4,5] for all atoms as implemented in *Gaussian 16* rev. B.01.[6] Single point (SP) corrections were performed using M06-2X functional and def2-TZVP[4] basis set for all atoms. The implicit SMD continuum solvation model[7] was used to account for the solvent effect of dichloromethane ($CH_2Cl_2$) on the conformer free energies. Gibbs energies were evaluated at the room temperature, as was used in the experiments, using a quasi-RRHO treatment of vibrational entropies.[8,9] Vibrational entropies of frequencies below 100 $cm^{-1}$ were obtained according to a free rotor description, using a smooth damping function to interpolate between the two limiting descriptions. The free energies were further corrected using standard concentration of 1 mol/L, which was used in solvation calculations. Conformer Gibbs energies evaluated at SMD(DCM)-M06-2X/def2-TZVP//M06-2X/def2-SVP level of theory are given and quoted in kcal $mol^{-1}$. (See section on conformational sampling for more details; *vide infra*).
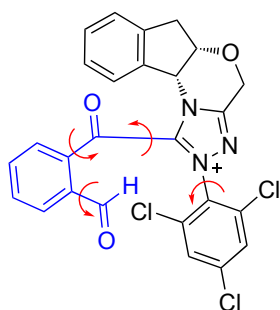
For reaction mechanistic studies, geometries are optimized in implicit SMD($CH_2Cl_2$) solvent at M06-2X/def2-SVP level of theory. Minima and transition structures on the potential energy surface (PES) were confirmed as such by harmonic frequency analysis, showing respectively zero and one imaginary frequency, at the same level of theory. The Gibbs energies obtained were further corrected with SMD($CH_2Cl_2$)-M06-2X/def2-TZVP single-point energy evaluations. The final SMD($CH_2Cl_2$)-M06-2X/def2-TZVP//SMD($CH_2Cl_2$)-M06-2X/def2-SVP energies are used for discussion of reaction mechanisms throughout the main text and in this supporting information.
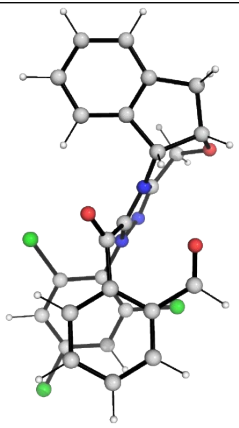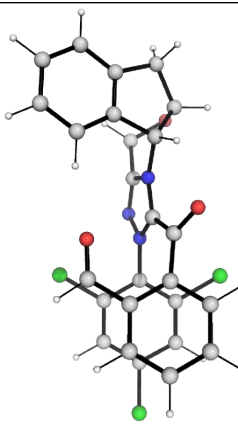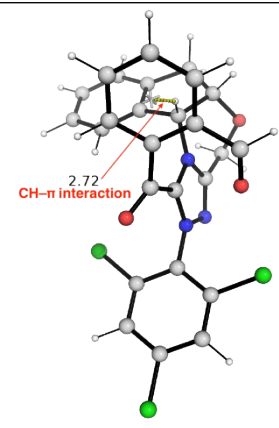
Non-covalent interactions (NCIs) were analyzed using NCIPLOT[10] calculations. The *.wfn* files for NCIPLOT were generated at M06-2X/def2-SVP level of theory. NCI indices calculated with NCIPLOT were visualized at a gradient isosurface value of *s = 0.5* au. These are colored according to the sign of the second eigenvalue ($\lambda_2$) of the Laplacian of the density ($\nabla^2\rho$) over the range of –0.1 (blue = attractive) to +0.1 (red = repulsive). Molecular orbitals are visualized using an isosurface value of 0.05 au throughout. All molecular structures and molecular orbitals were visualized using *PyMOL* software.[11]

## 1. Conformational considerations

To determine the most stable form of the key acyl azolium intermediate **II** involved in the reaction, we performed a thorough conformational sampling. We generated a set of rotamers by performing 5-fold rotations about four key dihedral angles (in red) as shown in the Chemdraw structure in Figure S3. This

set of total 625 rotamers were then cleaned by removing those species having overlapping atoms within 0.5 Å radius. These were performed using the script in the study of conformational effects on physical-organic descriptors by Brethomé *et al.*[12] A total of 52 resulting rotamers were then subject to geometry optimization using GFN1-xTB in Entos Qcore. The xTB-optimized structures were then clustered using the clustering_traj.py[13] with an RMSD cutoff of 1.0 Å (excluding H atoms) to give 6 distinct conformers, which were reoptimized at DFT M06-2X/def2-SVP level. The Gibbs energies of the resulting structures were corrected using single-point M06-2x/def2-TZVP in SMD($CH_2Cl_2$). Their relative solvent-corrected Gibbs energies are given in Figure S3. As would be expected, the most stable conformers (**II-c1** and **II-c2**) benefit from π–π interaction between the phenyl ring on imine substrate (**1a**) and the aryl ring on NHC ligand. Conformer **II-c3** is less stable as it loses the π–π interaction although it gains some CH–π interaction.



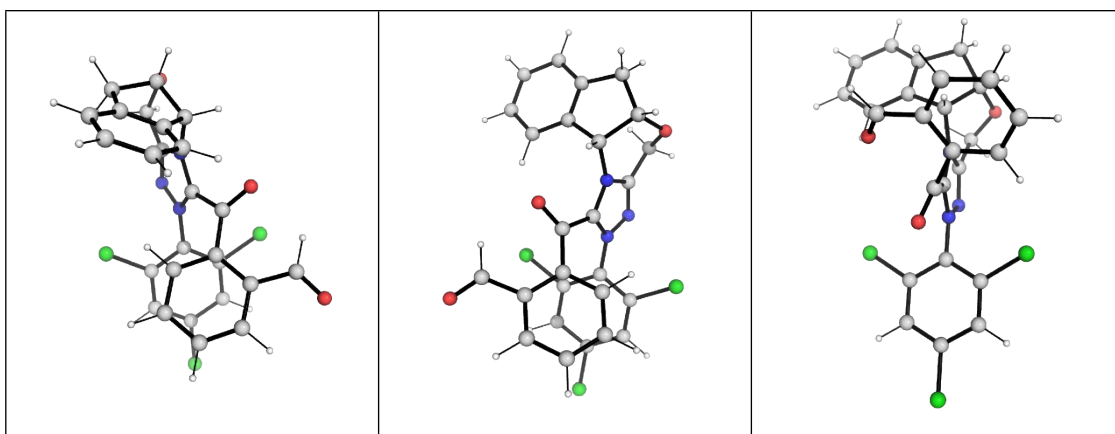| II-c1 | II-c2 | II-c3 |
|---|---|---|
| ΔΔG = 0.0 | 3.8 | 4.2 |
|  |  |  |
| II-c4 | II-c5 | II-c6 |
| ΔΔG = 4.8 | 5.4 | 6.5 |

**Figure S3**. Chemdraw and DFT optimized conformer structures of key acyl azolium intermediate **II**. Relative Gibbs energies are calculated at SMD(CH$_2$Cl$_2$)-M06-2X/def2-TZVP//M06-2X/def2-SVP level of theory. Their units are given in kcal mol$^{-1}$.

For subsequent calculations for mechanistic studies, the most stable conformers **II-c1** and **II-c2** are used for geometry optimization in implicit SMD(CH$_2$Cl$_2$) solvent and their Gibbs energies further corrected using single-point M06-2X/def2-TZVP energy in implicit SMD(CH$_2$Cl$_2$) solvent. Both of these conformers are involved in the stereoselective C–N bond formation as for each conformer, only one face is available for attack as their other face is shielded from attack by the 2,4,6-trichlorophenyl moiety of NHC. For example, conformer **II-c1** (also named *(Si)*-**II**) can only undergo *Si*-face attack as its *Re*-face is shielded; similarly, conformer **II-c2** (also named *(Re)*-**II**) can only undergo *Re*-face attack.

For N-phenyl benzenesulfonamide substrate, the X-ray crystal structure was taken from The Cambridge Crystallographic Data Centre (CCDC Number: 607421) as the initial structure for DFT geometry optimization.

## 2. Role of Li$^+$ ion in the reaction

First, we consider possible reaction pathways in which Li$^+$ ion does not participate directly, after deprotonation of N-phenyl benzenesulfonamide substrate by LiOH. For the reaction between the deprotonated sulfonamide and acyl azolium intermediate **II**, the reaction complex was first optimized in the solvent phase. Subsequently, a relaxed PES scan along the N-atom of the deprotonated sulfonamide and the carbonyl carbon of the acyl azolium intermediate **II** was performed in implicit CH$_2$Cl$_2$ solvent (scanning coordinate shown in Scheme S-1). These scans show that there is only a very small barrier (< 1 kcal mol$^{-1}$) for the attack of the amide anion to the aldehyde group in the absence of Li$^+$ ion (for both the *Re*-face attack, Figure S4(i) and the *Si*-face attack, Figure S4(ii)). The scans also show that once the C–N bond is formed, the subsequent oxyanion attacks into the adjacent carbonyl group directly, forming the cyclized product immediately without a barrier (Figure S4).
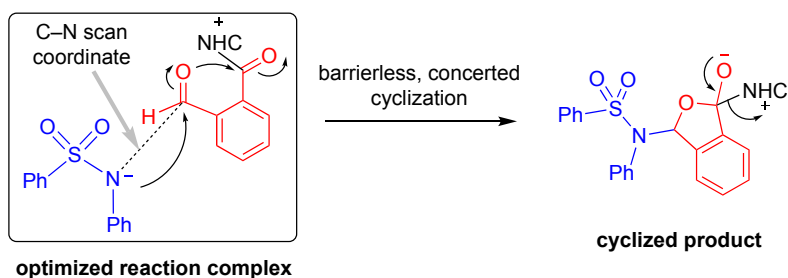
**Scheme S-1.** Reaction pathway between deprotonated sulfonamide and acyl azolium intermediate **II** in the absence of Li$^+$ ion (overall neutral reaction). The C–N coordinate for relaxed PES scan is shown.

The lack of a high activation barrier for the reaction between deprotonated sulfonamide anion and the positively charged acyl azolium intermediate is perhaps unsurprising as their reaction is highly favored by electrostatic interactions in dichloromethane solvent (low dielectric constant of 8.93; cf. dielectric constant of water = 80.4). Thus, in the absence of Li$^+$ ion, the product selectivity will be determined by the conformer distribution of the acyl azolium intermediate **II-c1** and **II-c2**. Since **II-c1** is more thermodynamically stable than **II-c2**, this mechanism (no Li$^+$ ion involvement) predicts that *Si*-face attack would be favored, which is inconsistent with experimental observation where the *Re*-face attack product is observed. Therefore, a mechanism involving the role of Li$^+$ ion is important for our consideration.

For completeness, the comparative Gibbs energy profiles for this mechanism without Li$^+$ ion involvement calculated at SMD(CH$_2$Cl$_2$)-M06-2X/def2-TZVP//SMD(CH$_2$Cl$_2$) -M06-2X/def2-SVP level of theory is show in Figure S5. From this free Gibbs energy profile, we can see that the addition of deprotonated sulfonamide into the *(Si)*-face has an overall barrier of 3.0 kcal mol$^{-1}$, arising from the loss of NHC from the cyclized product; the addition to the *(Re)*-face has a barrier of 6.1 kcal mol$^{-1}$. Thus, without Li$^+$ ion involvement, the reaction will favor the *(Si)*-face addition by 3.1 kcal mol$^{-1}$, translating to an enantioselective ratio (e.r.) of 99.5 : 0.5 in favor of *(R)*-phthalidyl sulfonamide product (see reference[14], for example, for computing enantioselectivity from DFT calculations). Therefore, without the participation of Li$^+$ ion, the opposite enantioselectivity will be observed as the conformer for *(Si)*-face is more thermodynamically stable and its cyclization and NHC regeneration are kinetically faster.
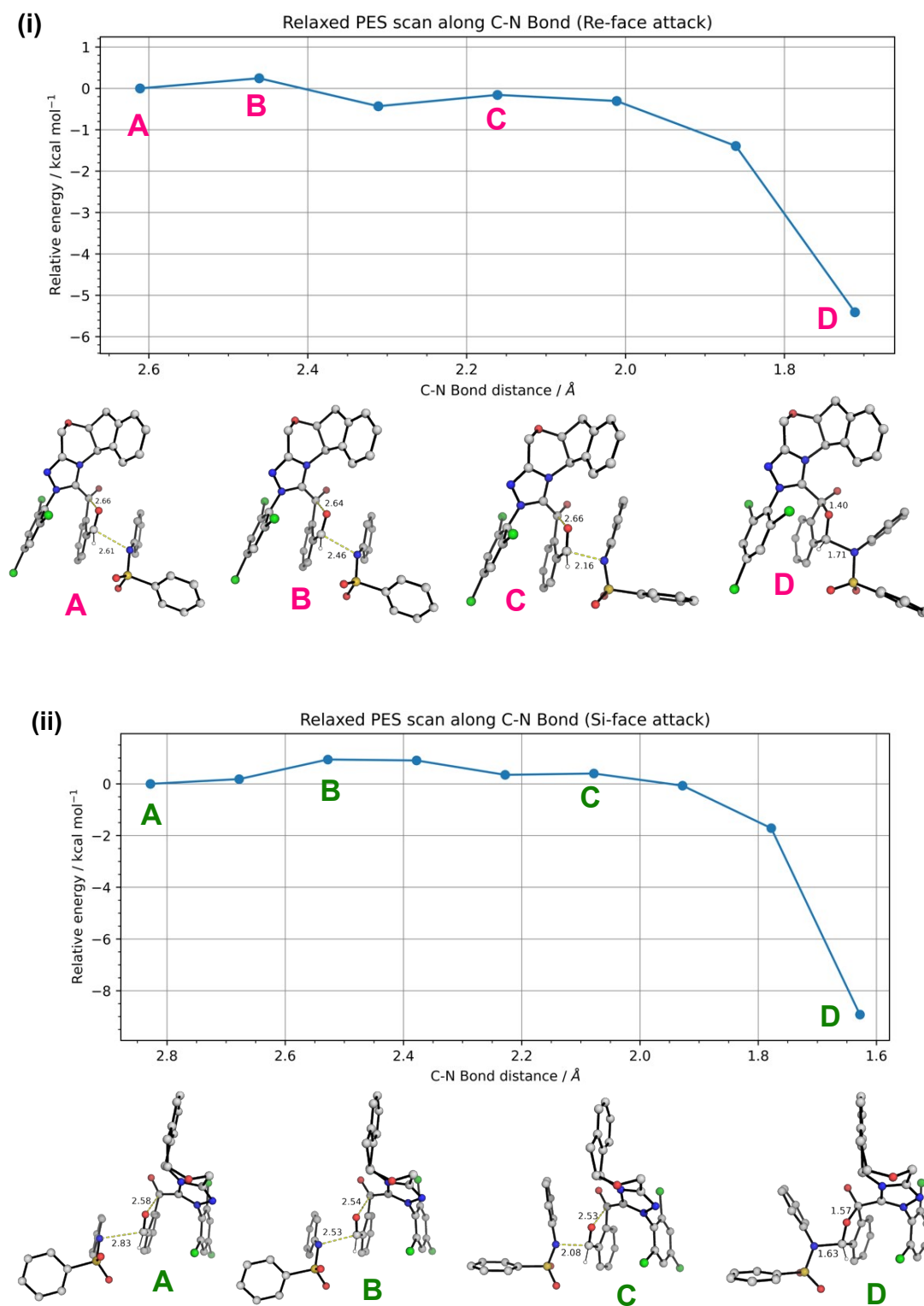
**Figure S4**. Relaxed potential energy surface (PES) scan for the first C–N bond formation for (i) *Re*-face attack and (ii) *Si*-face attack in the absence of $Li^+$ ion computed at $SMD(CH_2Cl_2)$-M06-2X/def2-SVP level of theory. Energies are taken relative to their respective reactant complexes (structures at point A) and their units are given in kcal mol^{-1}. These PES scans give an upper bound of C–N bond formation transition states (TSs) at < 1 kcal mol^{-1}, indicating very flat PES at this region in the absence of $Li^+$ ion.
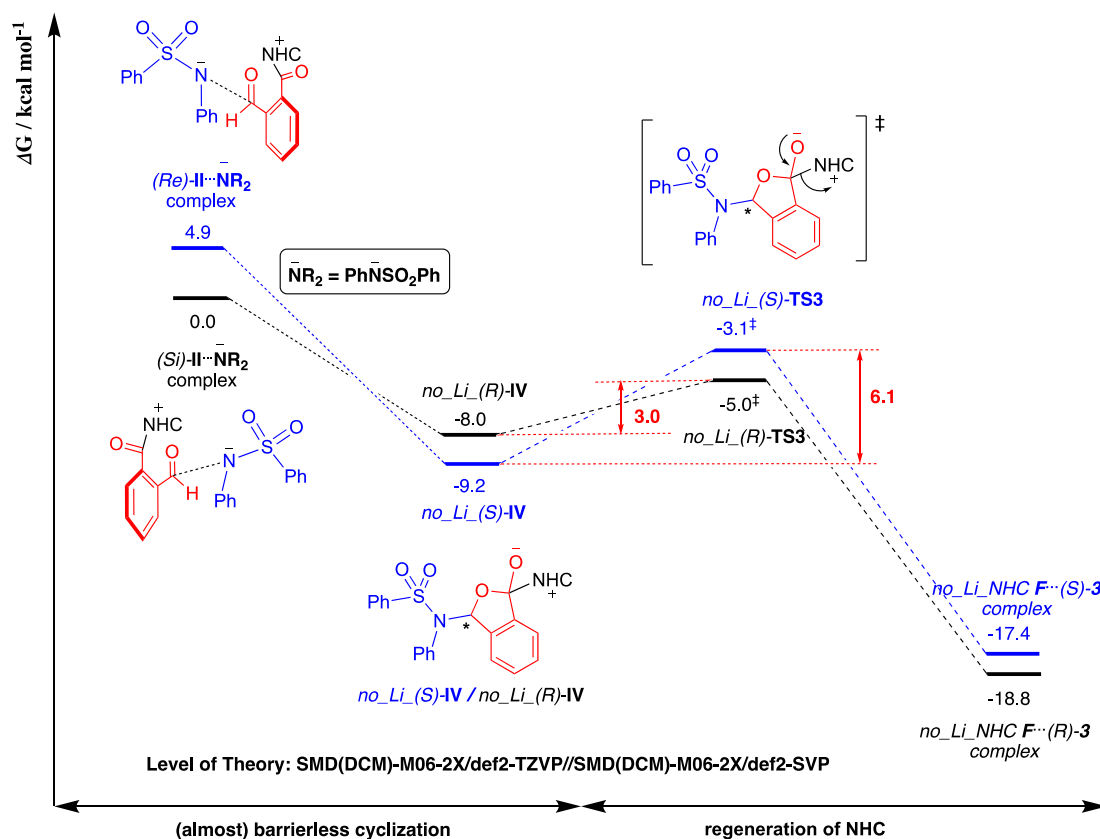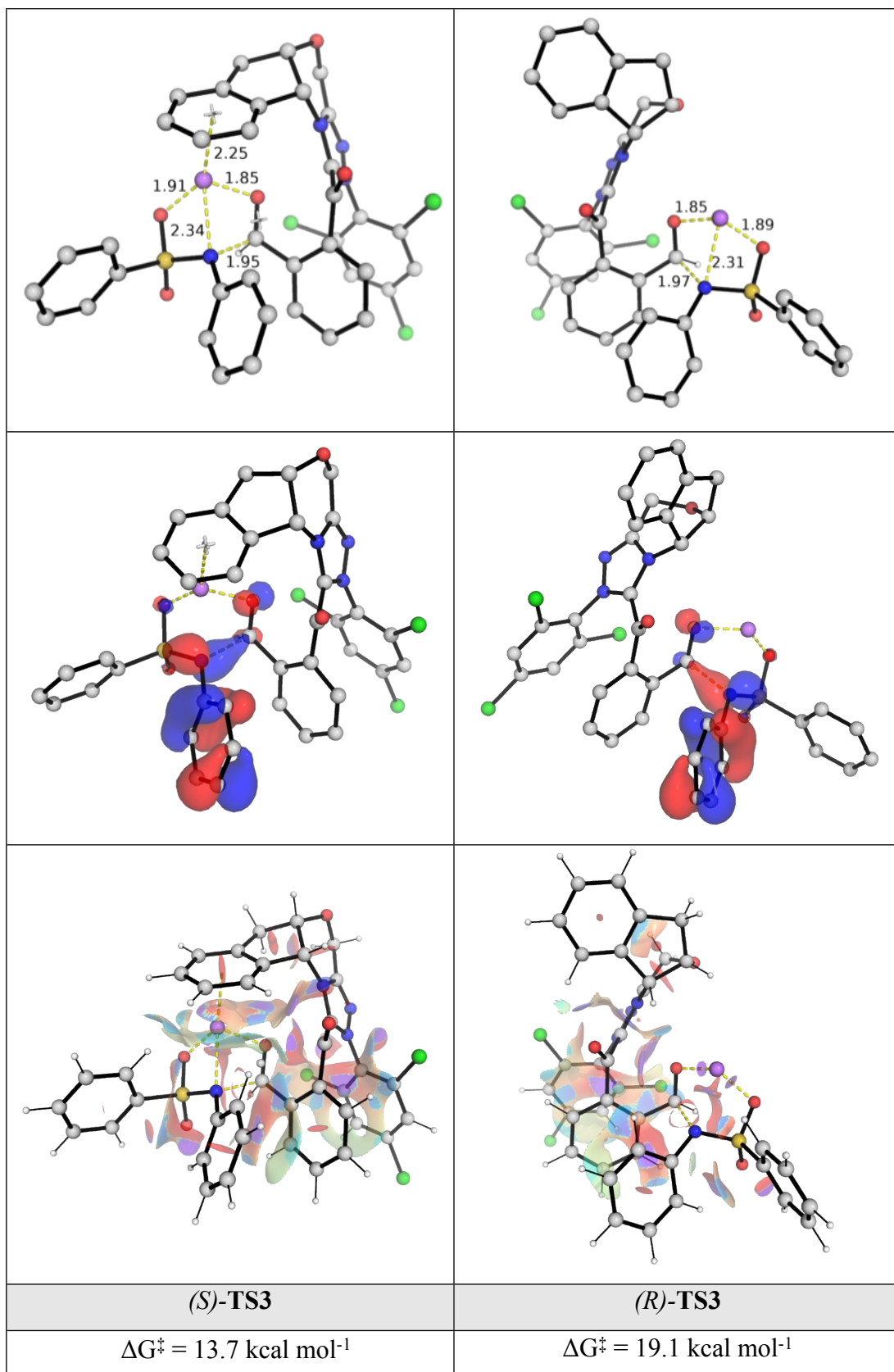
Figure S5. Gibbs energy profile computed at SMD($CH_2Cl_2$)-M06-2X/def2-TZVP// SMD($CH_2Cl_2$)- M06-2X/def2-SVP level of theory for the reaction between NHC-bound intermediate **II** and deprotonated sulfonamide in the absence of Li+ ion.

## 3. Key transition state (TS) structures with Li+ ion participation

For completeness, we compare the factors influencing the energetic differences between key TSs (*(Re)/(Si)*-**TS1** and *(Re)/(Si)*-**TS3**), although we note that **TS3**s are the turnover-frequency (TOF) determining transition state (TDTS).[15] Figure S6 shows their DFT-optimized structures, highest occupied molecular orbitals (HOMOs) and non-covalent interaction (NCI) plots.

For the formation of C–N bond in the first step (**TS1**), the addition to the *Re*-face is more favorable by 5.3 kcal mol$^{-1}$ due to more NCIs arising from the coordination of Li+ ion to the aromatic ring (cation-$\pi$ interaction). The electron distributions in their HOMOs are similar, as the lone pair nitrogen attacks into the $\pi$* orbital of the carbonyl group, indicating similar orbital interactions as the C–N bond is formed; the bond forming distances are also similar (1.95Å in *(Re)*-**TS1** and 1.97Å in *(Si)*-**TS1**; within 0.02 Å).

| *(Re)*-**TS1** | *(Si)*-**TS1** |
|---|---|
| $\Delta G^{\ddagger}$ = 8.0 kcal mol$^{-1}$ | $\Delta G^{\ddagger}$ = 13.3 kcal mol$^{-1}$ |

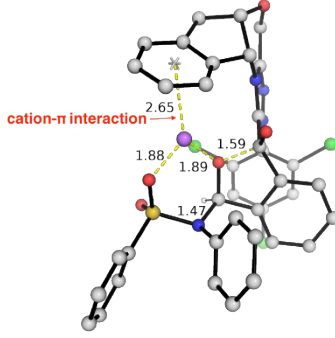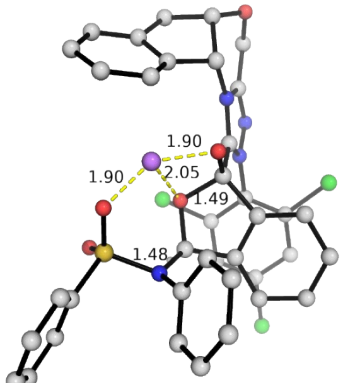| *(S)*-**TS3** | *(R)*-**TS3** |
|:---:|:---:|
| $\Delta G^{\ddagger} = 13.7$ kcal mol$^{-1}$ | $\Delta G^{\ddagger} = 19.1$ kcal mol$^{-1}$ |
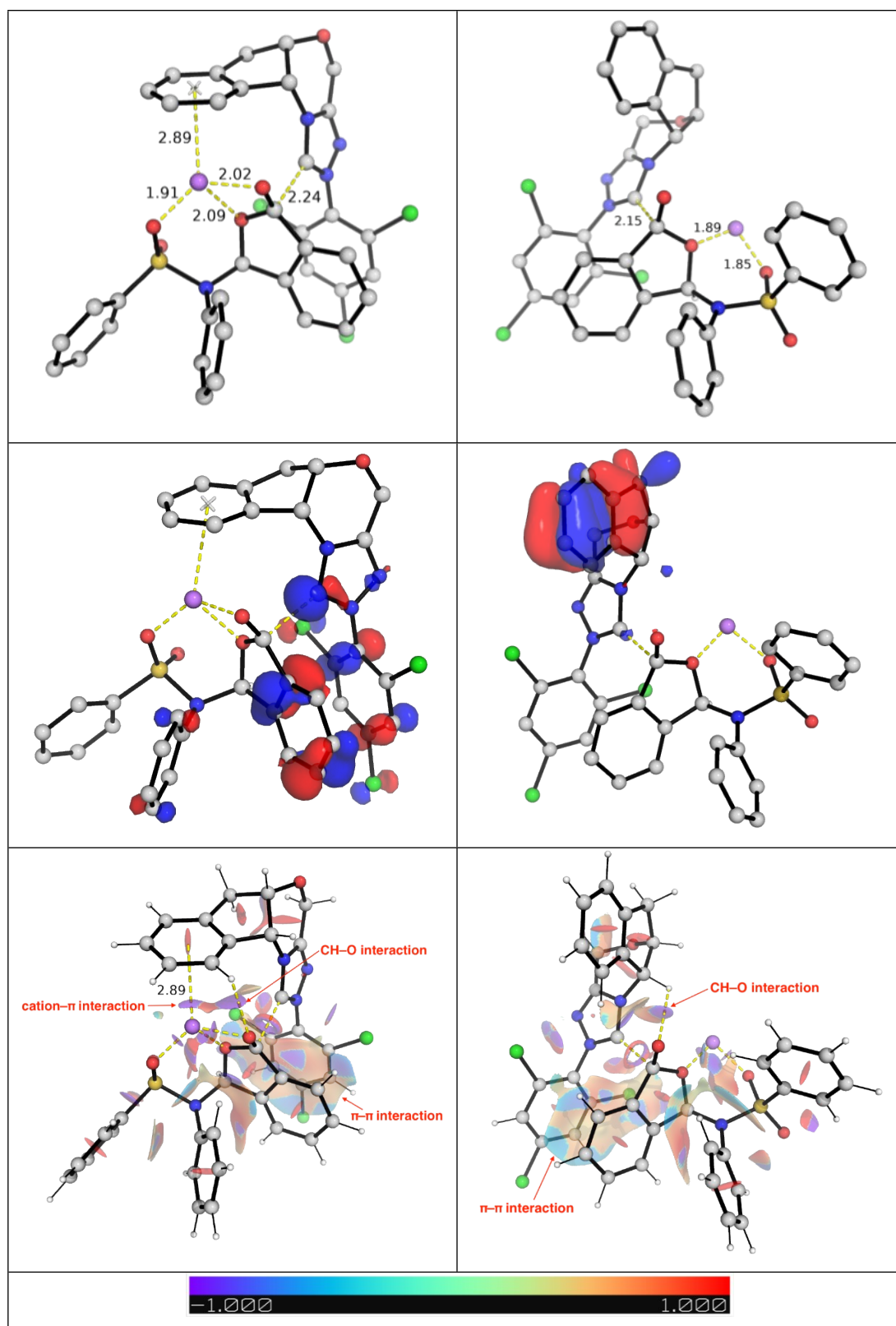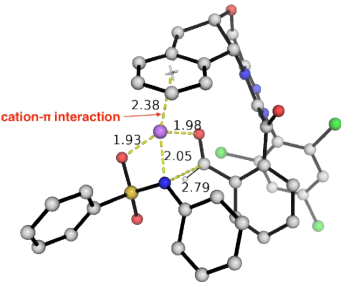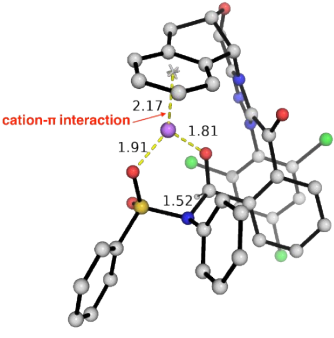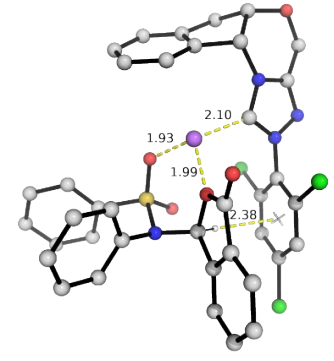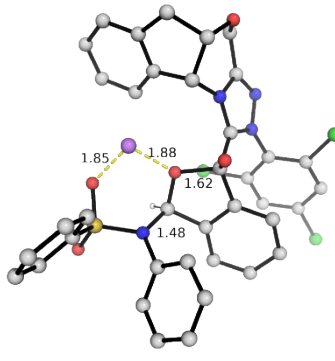
Figure S6. Optimized TS structures, their HOMO (isosurface value = 0.05 au) and NCI plots for the key transition states (TSs) for the reaction between acyl azolium intermediate **II** conformers **II-c1** (prone to *Si*-face attack) and **II-c2** (prone to *Re*-face attack) and lithium sulfonamide. Key bond distances are given in Å. Activation barriers are given in kcal mol^{-1}.

For the TDTSs, orbital interactions are more favorable in *(S)*-**TS3** than in *(R)*-**TS3**, as the σ*(C–C) orbital is directly involved in the HOMO of the former but not the latter. *(S)*-**TS3** is also a later transition state

as the breaking C–C bond distance (2.24Å) is much longer than that in *(R)*-**TS3** (2.15Å). The additional cation-π interaction in *(S)*-**TS3,** which is absent in *(R)*-**TS3**, further contributes to the stability of this TS (albeit diminished due to long Li–π distance of 2.89Å). Taken the orbital and non-covalent interactions together, *(S)*-**TS3** is lower in activation barrier than *(R)*-**TS3** by 5.4 kcal mol^{-1}.

The cation-π interaction in *(S)*-**TS3** is critical as the lack of it in another TS conformer, *(S)*-**TS3-c2** (Figure S7), gives a higher barrier (by 2 kcal mol^{-1}) than *(S)*-**TS3** where the cation-π interaction is present. The presence of cation-π interaction also stabilize the intermediate (**S-IV** vs **S-IV-c2**) and product complexes (**NHC-S-3-complex** vs **NHC-S-3-complex-c2**) by *ca.* 8–14 kcal mol^{-1} (Figure S7).

## 4. Other optimized structures with Li^{+} ion participation

| Re-II-Li-amide-complex | S-III | S-TS2 |
|---|---|---|
| ΔG = -1.6 | 1.9 | 4.9 |
|  |  |  |
| **S-IV** | **NHC-S-3-complex** | **S-IV-c2** |
| ΔG = 0.7 | -11.4 | 9.3 |
|  |  |  |
| **S-TS3-c2** | **NHC-S-3-complex-c2** | |
| ΔG = 15.7 | 3.4 | |
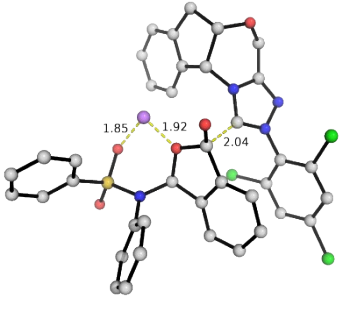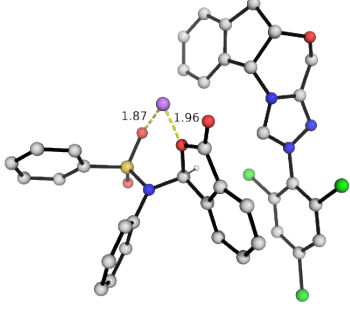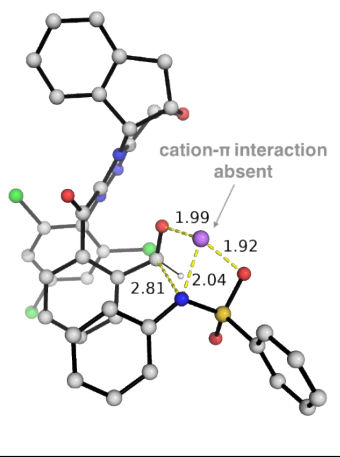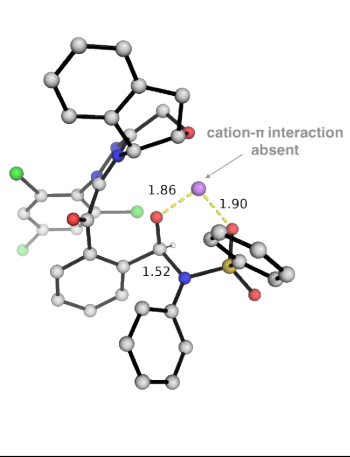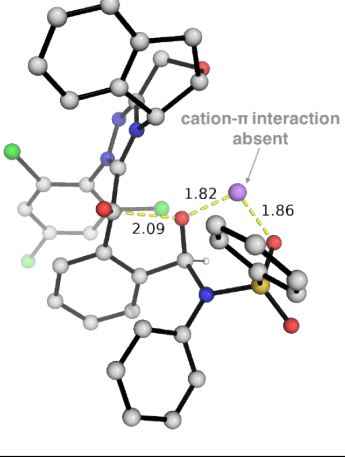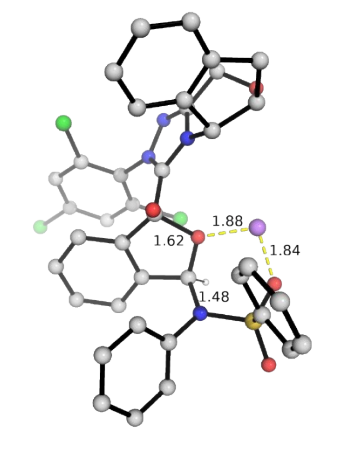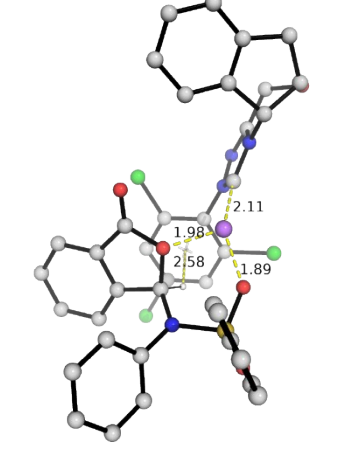
Figure S7. Other DFT-optimized structures for the reaction between acyl azolium intermediate and lithium sulfonamide. Key bond distances are given in Å. Gibbs energies are given in kcal mol$^{-1}$.

## 5. Use of DBU in place of Li$^+$ ion participation

When protonated DBU, **DBUH⁺**, is used in place of Li⁺ ion, it was found that the *(S)*-**TS3-DBU** is favored over *(R)*-**TS3-DBU** by 0.5 kcal mol⁻¹ (Figure S8). This calculated barrier difference in the TDTSs translates to an enantiomeric ratio (e.r.) of 70:30 for *S:R* enantiomeric products. We note that the experimentally observed e.r. of 86:14 corresponds to a barrier difference of 1.0 kcal mol⁻¹, which already falls into the heaven of chemical accuracy, making its exact agreement with computation difficult.

| *(S)*-**TS3-DBU** | *(R)*-**TS3-DBU** |
|---|---|
| $\Delta\Delta G^{\ddagger}$ = 0.0 kcal mol⁻¹ | $\Delta\Delta G^{\ddagger}$ = 0.5 kcal mol⁻¹ |
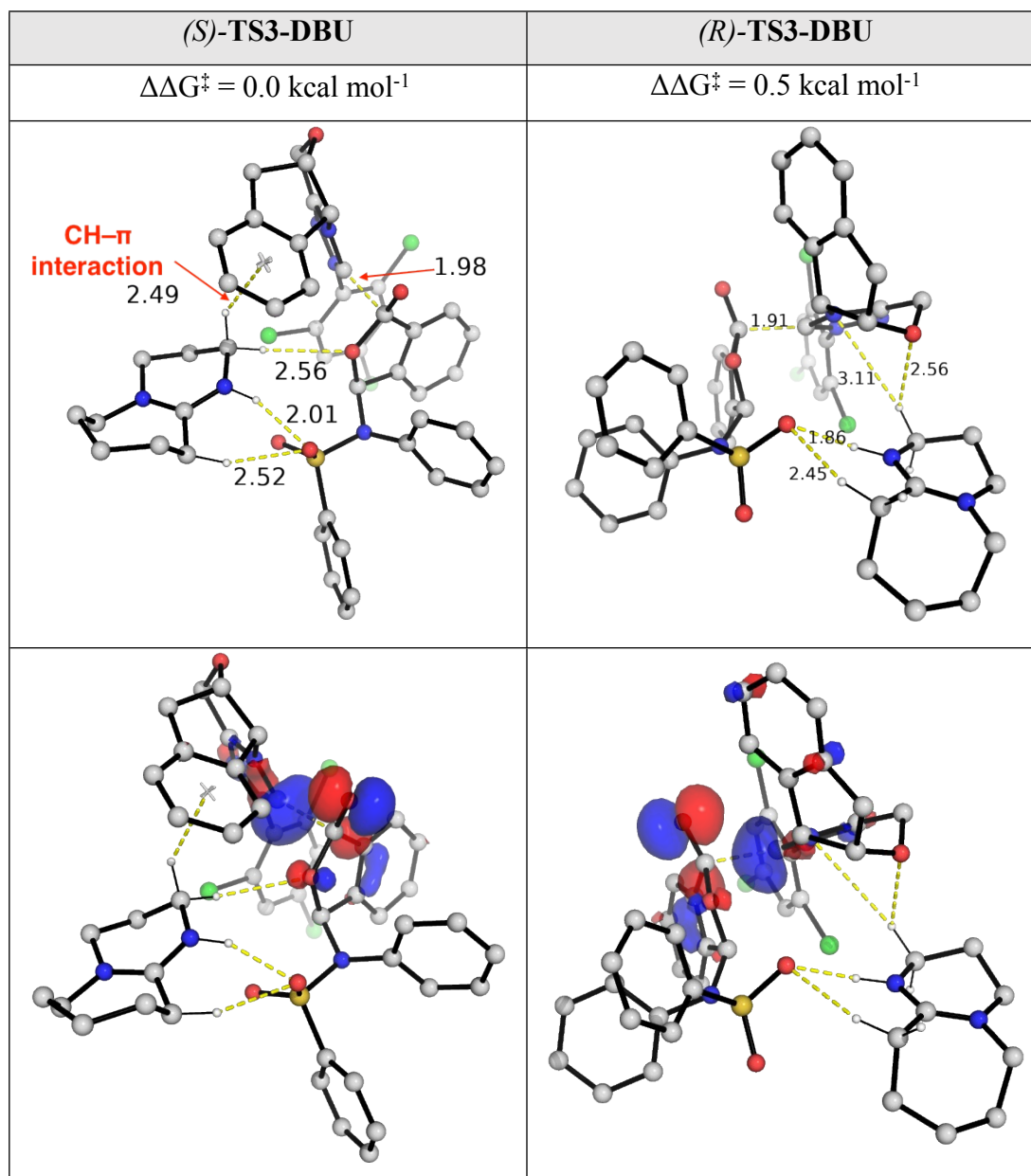


Figure S8. Optimized TS structures and their HOMO (isosurface value = 0.05 au) for the TDTSs with **DBUH⁺** in place of Li⁺ ion. Relative activation barriers are given in kcal mol⁻¹.

Our calculated value of 0.5 kcal mol⁻¹, although benefits from cancellation of errors, could still fall within the accuracy of the method. Thus, we can only conclude qualitatively that **DBUH⁺** can stabilize *(S)*-**TS3-**

**DBU** better than *(R)*-**TS3-DBU** (the TDTSs) in a way similar to, but less efficient than Li$^+$ ion (both TSs have similar HOMO structures).

## 6. Optimized structures and absolute energies, zero-point energies

Geometries of all optimized structures (in .xyz format with their associated energy in Hartrees) are included in a separate folder named *final_xyz_structures* with an associated readme.txt file. All these data have been deposited with this Supporting Information and uploaded to zenodo.org (DOI: 10.5281/zenodo.4409538).

Absolute values (in Hartrees) for SCF energy, zero-point vibrational energy (ZPE), enthalpy and quasi-harmonic Gibbs free energy (at 298.15K) for M06-2X/def2-SVP optimized conformers (intermediate **II-c1** to **II-c8**) and SMD(CH$_2$Cl$_2$)-M06-2X/ def2-SVP optimized structures (mechanistic study with and without Li$^+$ ion) are given below. Single point corrections in SMD(CH$_2$Cl$_2$) using M06-2X/def2-TZVP functional are also included.

| Structure | E/au | ZPE/au | H/au | T.S/au | qh-G/au | SP M06-2X/def2TZVP |
|---|---|---|---|---|---|---|
| **II-c1** | -2769.256458 | 0.385637 | -2768.8417 | 0.08733 | -2768.92275 | -2771.340557 |
| **II-c2** | -2769.253414 | 0.386164 | -2768.8385 | 0.085218 | -2768.918501 | -2771.335742 |
| **II-c3** | -2769.243215 | 0.385649 | -2768.8285 | 0.087561 | -2768.909579 | -2771.333778 |
| **II-c4** | -2769.242577 | 0.385917 | -2768.8276 | 0.0876 | -2768.908751 | -2771.33293 |
| **II-c5** | -2769.240971 | 0.385567 | -2768.8264 | 0.087169 | -2768.907342 | -2771.331798 |
| **II-c6** | -2769.240687 | 0.385521 | -2768.826 | 0.088955 | -2768.907782 | -2771.329355 |
| **Li_amide** | -1073.329428 | 0.200344 | -1073.114 | 0.054545 | -1073.166191 | -1074.272205 |
| **Si-II** | -2769.342222 | 0.385354 | -2768.9279 | 0.085587 | -2769.008202 | -2771.341036 |
| **Re-II** | -2769.339156 | 0.385754 | -2768.9247 | 0.084696 | -2769.004424 | -2771.336673 |
| **Re-II-Li-amide-complex** | -3842.708353 | 0.587944 | -3842.0761 | 0.122213 | -3842.186661 | -3845.640211 |
| **Re-TS1** | -3842.699114 | 0.588772 | -3842.0673 | 0.116579 | -3842.174502 | -3845.627887 |

| | | | | | | |
|---|---|---|---|---|---|---|
| **S-III** | -3842.714195 | 0.590206 | -3842.0818 | 0.114271 | -3842.187237 | -3845.639988 |
| **S-TS2** | -3842.711847 | 0.590289 | -3842.0797 | 0.113548 | -3842.184274 | -3845.63581 |
| **S-IV** | -3842.719735 | 0.591285 | -3842.0861 | 0.114823 | -3842.191653 | -3845.642986 |
| **S-TS3** | -3842.694656 | 0.588947 | -3842.0631 | 0.116576 | -3842.169613 | -3845.619147 |
| **NHC-S-3-complex** | -3842.733711 | 0.590231 | -3842.1 | 0.119146 | -3842.208212 | -3845.659601 |
| **S-IV-c2** | -3842.701179 | 0.590074 | -3842.0682 | 0.117425 | -3842.17549 | -3845.626864 |
| **S-TS3-c2** | -3842.689598 | 0.589207 | -3842.0578 | 0.117145 | -3842.164591 | -3845.616018 |
| **NHC-S-3-complex-c2** | -3842.7047 | 0.589239 | -3842.0715 | 0.121507 | -3842.181247 | -3845.634063 |
| **Si-II-Li-amide-complex** | -3842.697002 | 0.587348 | -3842.065 | 0.123577 | -3842.1765 | -3845.630373 |
| **Si-TS1** | -3842.687274 | 0.58813 | -3842.0558 | 0.118778 | -3842.164171 | -3845.617886 |
| **R-III** | -3842.709308 | 0.59123 | -3842.0751 | 0.117333 | -3842.182542 | -3845.63353 |
| **R-TS2** | -3842.703021 | 0.590378 | -3842.0705 | 0.11336 | -3842.175517 | -3845.629172 |
| **R-IV** | -3842.703356 | 0.590713 | -3842.0701 | 0.115463 | -3842.176214 | -3845.629255 |
| **R-TS3** | -3842.684893 | 0.589347 | -3842.0529 | 0.117596 | -3842.160044 | -3845.610463 |
| **NHC-R-3-complex** | -3842.729178 | 0.590089 | -3842.0954 | 0.120768 | -3842.204594 | -3845.656959 |
| **no_Li_Si-II-amide-complex** | -3835.212724 | 0.584256 | -3834.5848 | 0.122247 | -3834.70705 | -3834.694902 |
| **no_Li_R-IV** | -3835.24097 | 0.587907 | -3834.6115 | 0.113657 | -3834.72518 | -3834.715945 |
| **no_Li_R-TS3** | -3835.232057 | 0.585722 | -3834.6044 | 0.118847 | -3834.72326 | -3834.711082 |
| **no_Li_NHC-R-3-complex** | -3835.252354 | 0.5867 | -3834.6227 | 0.121032 | -3834.74377 | -3834.731136 |
| **no_Li_Re-II-amide-complex** | -3835.209936 | 0.584528 | -3834.582 | 0.120578 | -3834.70261 | -3834.691098 |

| | | | | | | |
|---|---|---|---|---|---|---|
| no_Li_S-IV | -3835.244744 | 0.587847 | -3834.6152 | 0.114793 | -3834.73003 | -3834.72 |
| no_Li_S-TS3 | -3835.232123 | 0.586677 | -3834.6039 | 0.115598 | -3834.71945 | -3834.708846 |
| no_Li_NHC-S-3-complex | -3835.246852 | 0.586745 | -3834.6171 | 0.123437 | -3834.74052 | -3834.726711 |
| S-TS3-DBU | -4297.283862 | 0.849318 | -4296.3815 | 0.141084 | -4296.508312 | -4300.716229 |
| R-TS3-DBU | -4297.283392 | 0.849507 | -4296.3807 | 0.14172 | -4296.507872 | -4300.71544 |

# VI. References

**Full reference for Gaussian software:**

Gaussian 16, Revision B.01, Frisch, M. J.; Trucks, G. W.; Schlegel, H. B.; Scuseria, G. E.; Robb, M. A.; Cheeseman, J. R.; Scalmani, G.; Barone, V.; Mennucci, B.; Petersson, G. A.; Nakatsuji, H.; Caricato, M.; Li, X.; Hratchian, H. P.; Izmaylov, A. F.; Bloino, J.; Zheng, G.; Sonnenberg, J. L.; Hada, M.; Ehara, M.; Toyota, K.; Fukuda, R.; Hasegawa, J.; Ishida, M.; Nakajima, T.; Honda, Y.; Kitao, O.; Nakai, H.; Vreven, T.; Montgomery Jr., J. A.; Peralta, J. E.; Ogliaro, F.; Bearpark, M.; Heyd, J. J.; Brothers, E.; Kudin, K. N.; Staroverov, V. N.; Kobayashi, R.; Normand, J.; Raghavachari, K.; Rendell, A.; Burant, J. C.; Iyengar, S. S.; Tomasi, J.; Cossi, M.; Rega, N.; Millam, J. M.; Klene, M.; Knox, J. E.; Cross, J. B.; Bakken, V.; Adamo, C.; Jaramillo, J.; Gomperts, R.; Stratmann, R. E.; Yazyev, O.; Austin, A. J.; Cammi, R.; Pomelli, C.; Ochterski, J. W.; Martin, R. L.; Morokuma, K.; Zakrzewski, V. G.; Voth, G. A.; Salvador, P.; Dannenberg, J. J.; Dapprich, S.; Daniels, A. D.; Farkas, Ö.; Foresman, J. B.; Ortiz, J. V; Cioslowski, J.; Fox, D. J. Gaussian, Inc., Wallingford CT, 2016.

(1)    Grimme, S.; Bannwarth, C.; Shushkov, P. A Robust and Accurate Tight-Binding Quantum Chemical Method for Structures, Vibrational Frequencies, and Noncovalent Interactions of Large Molecular Systems Parametrized for All Spd-Block Elements (Z = 1-86). *J. Chem. Theory Comput.* **2017**, *13* (5), 1989–2009.

(2)    Manby, F. R.; Miller, T. F.; Bygrave, P. J.; Ding, F.; Dresselhaus, T.; Buccheri, A.; Bungey, C.; Lee, S. J. R.; Meli, R.; Steinmann, C.; et al. Entos : A Quantum Molecular Simulation Package. *ChemRxiv.* **2019**.

(3)    Zhao, Y.; Truhlar, D. G. The M06 Suite of Density Functionals for Main Group Thermochemistry, Thermochemical Kinetics, Noncovalent Interactions, Excited States, and Transition Elements: Two New Functionals and Systematic Testing of Four M06-Class Functionals and 12 Other Function. *Theor. Chem. Acc.* **2008**, *120* (1), 215–241.

(4)    Weigend, F.; Ahlrichs, R. Balanced Basis Sets of Split Valence, Triple Zeta Valence and

Quadruple Zeta Valence Quality for H to Rn: Design and Assessment of Accuracy. *Phys. Chem. Chem. Phys.* **2005**, *7* (18), 3297–3305.

(5)     Weigend, F. Accurate Coulomb-Fitting Basis Sets for H to Rn. *Phys. Chem. Chem. Phys.* **2006**, *8* (9), 1057–1065.

(6)     Frisch, M. J. .; Trucks, G. W. .; Schlegel, H. B. .; Scuseria, G. E. .; Robb, M. A. .; Cheeseman, J. R. .; Scalmani, G. .; Barone, V. .; Petersson, G. A. .; Nakatsuji, H. .; et al. Gaussian 16, Revision B.01. 2016.

(7)     Marenich, A. V.; Cramer, C. J.; Truhlar, D. G. Universal Solvation Model Based on Solute Electron Density and on a Continuum Model of the Solvent Defined by the Bulk Dielectric Constant and Atomic Surface Tensions. *J. Phys. Chem. B* **2009**, *113* (18), 6378–6396.

(8)     Grimme, S. Supramolecular Binding Thermodynamics by Dispersion-Corrected Density Functional Theory. *Chem.: Eur. J.* **2012**, *18* (32), 9955–9964.

(9)     Funes-Ardoiz, I.; Paton, R. S. GoodVibes v1.0.1 http://doi.org/10.5281/zenodo.56091.

(10)    Contreras-García, J.; Johnson, E. R.; Keinan, S.; Chaudret, R.; Piquemal, J. P.; Beratan, D. N.; Yang, W. NCIPLOT: A Program for Plotting Noncovalent Interaction Regions. *J. Chem. Theory Comput.* **2011**, *7* (3), 625–632.

(11)    Schrödinger, L. *The PyMOL Molecular Graphics Development Component, Version 1.8*; 2015.

(12)    Brethomé, A. V.; Fletcher, S. P.; Paton, R. S. Conformational Effects on Physical-Organic Descriptors: The Case of Sterimol Steric Parameters. *ACS Catal.* **2019**, *9* (3), 2313–2323.

(13)    Cezar, H. M. Clustering Traj https://github.com/hmcezar/clustering-traj.

(14)    Peng, Q.; Duarte, F.; Paton, R. S. Computing Organic Stereoselectivity - from Concepts to Quantitative Calculations and Predictions. *Chem. Soc. Rev.* **2016**, *45* (22), 6093–6107.

(15)    Kozuch, S.; Shaik, S. How to Conceptualize Catalytic Cycles? The Energetic Span Model. *Acc. Chem. Res.* **2011**, *44* (2), 101–110.

# VII. Characterization of products



**3a**